Fracture analysis of magnetoelectroelastic solids by using path independent integrals

W.Y. TIAN and R.K.N.D. RAJAPAKSE*
Department of Mechanical Engineering, The University of British Columbia, Vancouver, Canada V6T 1Z4
Author for correspondence (E-mail: rajapakse@mech.ubc.ca)

Abstract. A solution scheme based on the fundamental solution for a generalized edge dislocation in an infinite magnetoelectroelastic solid is presented to analyze problems involving single, multiple and slowly growing impermeable cracks. The fundamental solution for a generalized dislocation is obtained by extending the complex potential function formulation used for anisotropic elasticity. The solution for a continuously distributed dislocation is derived by integrating the solution for an edge dislocation. The problem of a system of cracks subjected to remote mechanical, electric and magnetic loading is formulated in terms of set of singular integral equations by applying the principle of superposition and the solution for a continuously distributed dislocation. The singular integral equation system is solved by using a numerical integration technique based on Chebyshev polynomials. The J_i and M-integrals for single crack and multi-cracks problems are derived and their dependence on the coordinate system is investigated. Selected numerical results for the M-integral, total energy release rate and mechanical energy release rate are presented for single, double and multiple crack problems. The case of a slowly growing crack interacting with a stationary crack is also considered. It is found that M-integral presents a reliable and physically acceptable measure for assessment of fracture behaviour and damage of magnetoelectroelastic materials.

1. Introduction

Modern materials such as magnetoelectroelastic solids are used in the development of smart structures technology. Magnetoelectroelastic composites (e.g. ferrite-ferroelectric composites) can be used to develop broadband sensing and actuating devices required in advanced engineering applications. Basic understanding of fracture behaviour of this class of materials is required before investigating more complex issues such as domain effects on fracture and magneto-electric fatigue. Unlike in the case of elastic materials, fracture problems in piezoelectric and magnetoelectroelastic materials involve some fundamental issues that are not yet resolved. For example, there is no consensus on the electric boundary conditions (permeable/conducting/insulating/presence of free charges) of a crack in a piezoelectric material and the role of electric loading on crack propagation. McHenry and Koepke (1983) observed that both positive and negative electric fields enhanced crack propagation. Compact tension tests performed by Park and Sun (1995), however, revealed that a positive electric field along the poling direction reduced the fracture load, while a negative electric

field increased it. Singh and Wang (1995) observed that crack propagation was inhibited by a positive applied electric field and enhanced by a negative field. Different fracture criteria (e.g. total energy release rate, mechanical energy release rate, strain energy density criterion, etc) when applied to piezoelectric materials predict different behaviour and crack propagation paths. Many of these issues applicable to piezoelectric solids are also relevant to magnetoelectroelastic solids although both experimental and theoretical studies involving fracture of magnetoelectroelastic materials are very limited.

O'Handley (2000) presents a comprehensive treatment of principles and applications of modern magnetic materials. These materials are generally categorized into two groups: soft and hard magnetic materials based on the magnitude of the coercive field. Parton and Kudryavtsev (1988) presented the basic theory of linear electromagnetoelasticity and referred to some early studies of this class of materials. The linear theory is applicable only to weakly magnetizable materials without hysteresis and domain effects. Shindo (1983), Shindo et al. (1999) and Shindo (2001) considered crack problems in soft ferromagnetic solids. Sabir and Maugin (1996) studied energy release rate of a crack in paramagnetic and soft ferromagnetic materials in the absence of hysteresis and spin-ordering effects. Fomethe and Maugin (1998) examined the driving force acting on a straight crack in an elastic hard ferromagnetic material by relating the driving force to a global material force (Maugin, 1995) and evaluating the energy release rate. They showed that path independent integrals such as the J-integral hold only when both material and spin inertia are neglected.

More recently, Liu et al. (2001) derived the Green's functions for an infinite magnetoelectroelastic plane containing an elliptic cavity. They reduced the cavity solution to obtain the solution for a permeable crack. Gao et al. (2003a, b) and Song and Sih (2003) analyzed single and collinear cracks and presented solutions for either the crack-tip Stress Intensity Factor (SIF) or the Strain Energy Density (SED) criterion. Liu et al. (2001) and Gao et al. (2003a, b) did not present any numerical results and it is difficult to obtain from their solutions dependence of fracture parameters on crack orientation and electric, magnetic and mechanical loading. Furthermore, it is known that damage development in brittle materials is characterized by the initiation and accumulation of multiple, arbitrarily oriented interacting cracks rather than a single crack or collinear cracks. In addition, the conventional crack-tip fracture parameters, such as the SIF and SED are known to have certain deficiencies when applied to assess situations involving a cluster of randomly distributed cracks (Tian and Chen, 2002).

Over the past 40 years, many path-independent integrals such as the J-integral, the J_k vectors, the L-integral, and the M-integral (Rice, 1968; Knowles and Sternberg, 1972; Budiansky and Rice, 1973; Chen and Lu, 2003) have been proposed to study behaviour of cracks. These path-independent integrals were first applied to single crack problems. Recently, the M-integral was employed to study multi-crack interaction problems in brittle elastic materials (Chen, 2001a; Tian and Chen, 2002). It is found that in comparison to crack-tip based fracture criteria such as the SIF and SED, the M-integral presents a better physical representation of fracture behaviour and provide an effective measure in assessing damage level due to clusters of arbitrarily distributed and strongly interacting micro-cracks. A review of literature indicates that application of path independent integrals to study fracture

magnetoelectroelastic solids has not received attention in the past. It should be noted that path independent integrals are valid only for weakly magnetizable materials without hysteresis and domain effects.

The objective of this paper is to conduct a comprehensive theoretical study of fracture problems in magnetoelectroelastic solids. Attention is focused on the application of the M-integral to examine impermeable single cracks, randomly distributed multiple impermeable cracks and slowly growing impermeable cracks. Solutions for the M-integral are compared with other fracture parameters such as the crack-tip total energy release rate and mechanical strain energy release rate. The analysis starts with the derivation of the fundamental solution for a continuously distributed generalized dislocation in an infinite magnetoelectroelastic plane. The formulation used in this paper is based on the continuously distributed dislocation model proposed by Gross (1982) for elastic materials. Using the fundamental solution for a distributed dislocation and the principle of superposition, the problems involving multiple cracks are formulated in terms of a system of singular integral equations. The solutions for SIFs, K_I and K_II, the Electric Displacement Intensity Factor (EDIF), K_E, the Magnetic Induction Intensity Factor (MIIF), K_M, as well as the total and mechanical strain energy release rates are presented. The J_i and M-integrals for single crack and multiple cracks problems are presented and their dependence on the reference coordinate system is examined. A proof of the conservation law of the J_i integral for magnetoelectroelastic solids is given. Selected numerical results are presented to portray the effects of crack orientation with respect to polarization, crack interaction, and electric, magnetic and mechanical loading on fracture parameters, and the merits of the M-integral are discussed. Accuracy of numerical results is also verified by using the conservation law of the J-integral.

2. Solution for a continuously distributed dislocation

2.1. FIELD EQUATIONS AND GENERAL SOLUTION

Linear response of a magnetoelectroelastic solid is governed by the following equations defined with respect to a standard Cartesian coordinate system (Parton and Kudryavtsev, 1988).

$$\sigma_{ij} = C_{ijkl}\varepsilon_{kl} - e_{lij}E_l - h_{lij}H_l,$$

$$D_i = e_{ikl}\varepsilon_{kl} + \omega_{il}E_l + \alpha_{il}H_l,$$

$$B_i = h_{ikl}\varepsilon_{kl} + \alpha_{il}E_l + \gamma_{il}H_l, \tag{1}$$

$$\varepsilon_{ij} = \tfrac{1}{2}(u_{i,j} + u_{j,i}), \quad E_i = -\phi_{,i} \quad H_i = -\varphi_{,i}, \tag{2}$$

$$\sigma_{ij,i} = 0, \quad D_{i,i} = 0, \quad B_{i,i} = 0, \tag{3}$$

where σ_{ij}, D_i, B_i, ε_{ij}, E_l, H_l, u_i, ϕ and φ are the stress, electric displacement, magnetic induction, strain, electric field, magnetic field, elastic displacements, electric potential and magnetic potential, respectively; ω_{il} and γ_{il} represent the dielectric permittivities and magnetic permeabilities, respectively; C_{ijkl}, e_{lij}, h_{lij}, and α_{il} denote the elastic, piezoelectric, piezomagnetic and electromagnetic constants, respectively.

Consider plane problems where the elastic displacements, electric potential and magnetic potential are functions of only x_1 and x_2 coordinates. In addition, the medium is assumed to be poled in the x_2 direction. Following Stroh (1958) and Ting (1996), the magnetoelectroelastic field can be expressed in terms of four complex-valued functions $f_1(z_1)$, $f_2(z_2)$, $f_3(z_3)$ and $f_4(z_4)$, where $z_j = x_1 + \mu_j x_2$ and μ_j is a complex parameter defined later. The general solutions for the in-plane displacements u_1 and u_2, electric potential ϕ, magnetic potential φ, stresses σ_{11}, σ_{12} and σ_{22}, electric displacements D_1 and D_2, and magnetic inductions B_1 and B_2 can be expressed in terms of $f_j(z_j)$ as,

$$\{u_i\} = 2\mathrm{Re}\left[\sum_{j=1}^{4} A_{ij} f_j(z_j)\right], \tag{4}$$

$$\{\Sigma_{2i}\} = 2\mathrm{Re}\left[\sum_{j=1}^{4} L_{ij} f_j'(z_j)\right], \quad \{\Sigma_{1i}\} = -2\mathrm{Re}\left[\sum_{j=1}^{4} L_{ij} \mu_j f_j'(z_j)\right], \tag{5}$$

where the generalized displacement vector, $\{u_i\} = \{u_1, u_2, \phi, \varphi\}^\mathrm{T}$; generalized stress vector in the x_1 direction, $\Sigma_1 = \{\sigma_{11}, \sigma_{12}, D_1, B_1\}^\mathrm{T}$; generalized stress vector in the x_2 direction, $\Sigma_2 = \{\sigma_{12}, \sigma_{22}, D_2, B_2\}^\mathrm{T}$; and $(\ )'$ denotes differentiation with respect to z_j.

In addition, $\mu_j (j = 1, 2, \ldots, 4)$ denotes the four eigenvalues (four distinct conjugate pairs with positive imaginary parts) and A_{ij} and L_{ij} denote the elements of the eigenvectors of the following eigenvalue problem.

$$\begin{bmatrix} -\mathbf{T}^{-1}\mathbf{\Pi}^\mathrm{T} & \mathbf{T}^{-1} \\ \mathbf{\Pi}\mathbf{T}^{-1}\mathbf{\Pi}^\mathrm{T} - \mathbf{\Lambda} & [-\mathbf{T}^{-1}\mathbf{\Pi}^\mathrm{T}]^\mathrm{T} \end{bmatrix} \begin{Bmatrix} \mathbf{a} \\ \mathbf{b} \end{Bmatrix} = \mu \begin{Bmatrix} \mathbf{a} \\ \mathbf{b} \end{Bmatrix}, \tag{6}$$

where

$$\mathbf{a}_j = \{A_{1j}, A_{2j}, A_{3j}, A_{4j}\}, \quad \mathbf{b}_j = \{L_{1j}, L_{2j}, L_{3j}, L_{4j}\}, \tag{7}$$

$$\mathbf{\Lambda} = \begin{bmatrix} C_{11} & 0 & 0 & 0 \\ 0 & C_{66} & e_{16} & h_{16} \\ 0 & e_{16} & -\omega_{11} & -\alpha_{11} \\ 0 & h_{16} & -\alpha_{11} & -\gamma_{11} \end{bmatrix} \quad \mathbf{\Pi} = \begin{bmatrix} 0 & C_{12} & e_{21} & h_{21} \\ C_{66} & 0 & 0 & 0 \\ e_{16} & 0 & 0 & 0 \\ h_{16} & 0 & 0 & 0 \end{bmatrix} \quad \mathbf{T} = \begin{bmatrix} C_{66} & 0 & 0 & 0 \\ 0 & C_{22} & e_{22} & h_{22} \\ 0 & e_{22} & -\omega_{22} & -\alpha_{22} \\ 0 & h_{22} & -\alpha_{22} & -\gamma_{22} \end{bmatrix}, \tag{8}$$

where C_{11}, e_{11}, etc are material constants and plane strain deformation is assumed together with poling in the x_2 direction. The general constitutive relation given by Equation (1) is specialized in Appendix A for three-dimensional deformations of a medium poled in the x_2 direction [Equations (A.1)–(A.3)] and for plane strain deformations [Equations (A.4)–(A.6)].

2.2. CONTINUOUSLY DISTRIBUTED DISLOCATION

Assume that there exists a generalized edge dislocation at point **P** $(\hat{x}_1, \hat{x}_2)$ in an infinite magnetoelectroelastic plane as shown in Figure 1. Following Miller (1989),

the complex potential functions corresponding to the edge dislocation at **P** can be expressed as,

$$f'_j(z_j) = \frac{\rho_j}{z_j - \hat{z}_j} \quad (j = 1, 2, 3, 4), \tag{9}$$

where $\hat{z}_j = \hat{x}_1 + \mu_j \hat{x}_2$ and ρ_j are complex constants to be determined.

Around a loop surrounding the point **P**, the stresses, electric displacements and magnetic induction are self-equilibrated, and the mechanical displacement, electric potential and magnetic potential jumps associated with the dislocation are denoted by the extended Burgers vector $\Delta \mathbf{u} = (\Delta u_1, \Delta u_2, \Delta \phi, \Delta \varphi)$. The complex constants ρ_j are determined by solving the following equations.

$$\text{Im} \sum_{j=1}^4 L_{ij} \rho_j = -\frac{X_i}{4\pi} \quad (i = 1, 2, 3, 4), \tag{10a}$$

$$\text{Im} \sum_{j=1}^4 A_{lj} \rho_j = -\frac{\Delta u_l}{4\pi} \quad (l = 1, 2), \tag{10b}$$

$$\text{Im} \sum_{j=1}^4 A_{3j} \rho_j = -\frac{\Delta \phi}{4\pi}, \quad \text{Im} \sum_{j=1}^4 A_{4j} \rho_j = -\frac{\Delta \varphi}{4\pi}, \tag{10c}$$

where X_1, and X_2 represent the net force in the x_1 and x_2 directions around a loop surrounding the dislocation and X_3 and X_4 denote the net electric displacement and net magnetic induction on a loop surrounding the dislocation. For a standard dislocation, $X_i (i = 1, 2, 3, 4)$ are identical to zero.

Consider a continuously distributed dislocation field along a line segment Γ with orientation angle β and length $2a$ (Figure 1). A local coordinate ξ is defined along Γ with its origin at the centre point $Q(x_1^0, x_2^0)$ of Γ. Let the generalized Burgers vector of the dislocation field along Γ be denoted by $\Delta \mathbf{u}(\xi) = (\Delta u_1(\xi), \Delta u_2(\xi), \Delta \phi(\xi), \Delta \varphi(\xi))$. Then along Γ, $z = x_1^0 + ix_2^0 + \xi e^{i\beta}$, and $i = \sqrt{-1}$, $-a < \xi < a$. The solution for magnetoelectroelastic field due to a dislocation of intensity $\Delta \mathbf{u}(\xi)$ at point **P** is given by the Equation (9) with ρ_j replaced by $\rho_j(\xi)$. Coupled field corresponding to the distributed dislocation field on Γ can therefore be expressed in terms of the complex potential functions $f_j(z_j)$ defined by,

$$f'_j(z_j) = \int_{-a}^a \frac{\rho_j(\xi)}{z_j - \hat{z}_j(\xi)} \mathrm{d}\xi. \tag{11}$$

Consider a point $R(x_1, x_2)$ as shown in Figure 1, and define another Cartesian coordinate system (x_1', x_2') with the origin at R and orientation angle β_1 with respect to x_1. Let the generalized stress vector in the x_2' direction at an arbitrary point S $(z = x_1 + ix_2 + \eta e^{i\beta_1})$ due to the distributed dislocation field on Γ be denoted by $\Sigma_2' = \{\sigma_{21}', \sigma_{22}', D_2', B_2'\}^{\mathrm{T}}$. In view of Equations (5) and (11),

$$\Sigma_{2i}' = \int_{-a}^a 2\text{Re} \sum_{j=1}^4 \left[F_{ij}(\mu_j, \beta_1) \frac{\rho_j(\xi)}{\Psi(x_1^0, x_2^0, \xi, \beta, x_1, x_2, \eta, \beta_1, \mu_j)} \right] \mathrm{d}\xi, \quad (i = 1, 2, 3, 4) \tag{12}$$
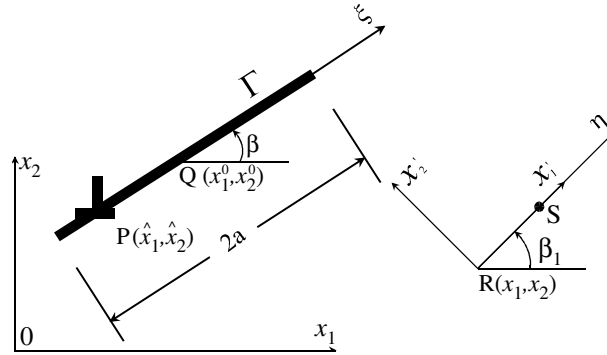
Figure 1. Coordinate system and geometry of continuously distributed dislocation.

where η is a local coordinate defined as shown in Figure 1 and

$$F_{1j}(\mu_j, \beta_1) = \tfrac{1}{2}(L_{1j}\mu_j + L_{2j})\sin 2\beta_1 + L_{1j}\cos 2\beta_1 \tag{13a}$$

$$F_{2j}(\mu_j, \beta_1) = -L_{1j}\mu_j \sin^2 \beta_1 + L_{2j}\cos^2 \beta_1 - L_{1j}\sin 2\beta_1 \tag{13b}$$

$$F_{lj}(\mu_j, \beta_1) = L_{lj}\mu_j \sin \beta_1 + L_{lj}\cos \beta_1 \quad (l = 3, 4) \tag{13c}$$

$$\Psi(x_1^0, x_2^0, \xi, \beta, x_1, x_2, \eta, \beta_1, \mu_j) = x_1 - x_1^0 + \eta \cos \beta_1 - \xi \cos \beta$$
$$+ (x_2 - x_2^0 + \eta \sin \beta_1 - \xi \sin \beta)\mu_j. \tag{13d}$$

3. Formulation of multiple cracks problem

Gross (1982) developed a method to analyze cracks in an ideal elastic medium by considering them as continuously distributed dislocations. Gross' approach was extended for piezoelectric materials by Xu and Rajapakse (2000) who solved the problem of a branched crack in a piezoelectric medium by using the basic solution for a generalized dislocation in an infinite piezoelectric solid. Consider an infinite magnetoelectroelastic solid with N arbitrarily oriented planar cracks as shown in Figure 2. All crack are assumed to be impermeable (i.e. electric displacement and magnetic induction normal to the crack faces are zero). A crack can be impermeable, permeable, semi-permeable or conducting with respect to the crack face electromagnetic boundary conditions. All these cases are practically possible depending on the geometry of the crack and the electromagnetic properties of the medium inside the crack. In experimental studies dealing with fracture of piezoelectric materials, the impermeable boundary condition has been justified by Park and Sun (1995) and Lynch et al. (1995). Furthermore, McMeeking (2001) presented an elegant discussion of crack face boundary conditions in piezoelectric materials and showed using theoretical arguments that the impermeable condition was often met in experiments. Although the above studies deal strictly with piezoelectric or dielectric materials it is reasonable to assume that the extension of the findings to electromagnetoelastic materials is valid. Domain switching effects caused by singular crack tip field is neglected in the present study as the development of domain switching models for the present class of materials is still in its infancy.
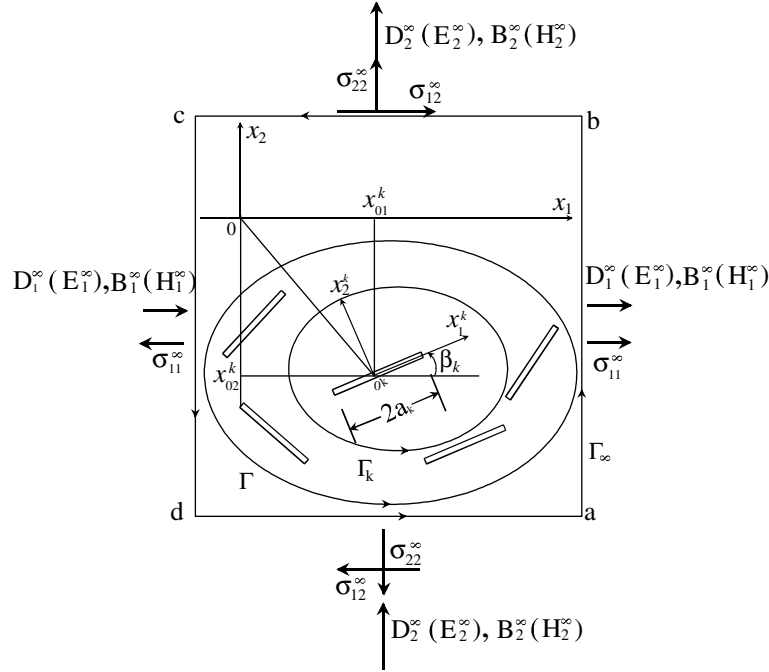
Figure 2. Geometry and loading system of a cluster of cracks.

The length and orientation angle of the kth crack ($k = 1, 2, \ldots, N$) are denoted by $2a_k$ and β_k, respectively. A global coordinate system (x_1, x_2) with the origin O and a local coordinate system (x_1^k, x_2^k) with the origin at the centre O^k of the kth crack are defined. A local coordinate ξ_k is defined along the length of the kth crack with its origin at O^k. The infinite plane containing the cracks is subjected to remote mechanical loading, σ_{11}^∞, σ_{12}^∞ and σ_{22}^∞, remote electric displacements D_2^∞ and D_1^∞ (or electric fields E_2^∞ and E_1^∞), and remote magnetic inductions B_2^∞ and B_1^∞ (or magnetic fields H_2^∞ and H_1^∞).

Following Gross (1982), each crack shown in Figure 2 can be modelled as a generalized distributed dislocation field of unknown density. The density of each dislocation field is such that the crack face boundary conditions [i.e., $\sigma_{2i}^k = 0$, ($i = 1, 2$), $D_2^k = 0$, $B_2^k = 0$] are satisfied under the far field loading shown in Figure 2. By using the solution for a distributed dislocation given by Equations (11) and (12) and the principle of superposition, the system shown in Figure 2 can be reduced to the following system of singular integral equations to determine the complex functions $\rho_j(\xi_k)$ related to the unknown distributed dislocation field corresponding to the kth crack.

$$2\mathrm{Re}\sum_{j=1}^{4}\left[F_{ij}(\mu_j, \beta_k)\left(\int_{-a_k}^{a_k} \frac{\rho_j(\xi_k)}{(\eta_k - \xi_k)(\cos\beta_k + \mu_j\sin\beta_k)}\mathrm{d}\xi_k \right.\right.$$

$$\left.\left. + \sum_{\substack{l=1 \\ l \neq K}}^{N} \int_{-a_i}^{a_i} \frac{\rho_j(\xi_l)}{\Psi(x_1^l, x_2^l, \xi_l, \beta_l, x_1^k, x_2^k, \eta_k, \beta_k, \mu_j)}\mathrm{d}\xi_l \right)\right] = p_i(\beta_k) \quad (i = 1, 2, 3, 4), \tag{14}$$

where $-a_k < \xi_k < a_k$, $-a_k < \eta_k < a_k$, and $p_i(\beta_k)$ $(i = 1, 2, 3, 4)$ can be expressed in terms of the magnitudes of the applied loading as,

$$
\begin{aligned}
p_1(\beta_k) &= -\left[(\sigma_{22}^\infty - \sigma_{11}^\infty)\cos\beta_k \sin\beta_k + \sigma_{12}^\infty \cos 2\beta_k\right] \\
p_2(\beta_k) &= -\left[\sigma_{11}^\infty \sin^2\beta_k + \sigma_{22}^\infty \cos^2\beta_k - \sigma_{12}^\infty \sin 2\beta_k\right] \\
p_3(\beta_k) &= -D_2^\infty \cos\beta_k + D_1^\infty \sin\beta_k \\
p_4(\beta_k) &= -B_2^\infty \cos\beta_k + B_1^\infty \sin\beta_k
\end{aligned}
\tag{15}
$$

In addition, the following constraint is required to ensure single-valued displacements (Erdogan, 1978).

$$
\int_{-a_k}^{a_k} \rho_j(\xi_k)\,d\xi_k = 0 \quad (k = 1, 2, \ldots, N). \tag{16}
$$

If the remote electric and magnetic loading corresponds to applied electric and magnetic fields instead of applied electric displacements and magnetic inductions, then $p_3(\beta_k)$ and $p_4(\beta_k)$ are given by,

$$
\begin{aligned}
p_3(\beta_k) &= -\left[(\mathbf{eC}^{-1}\mathbf{e}^{\mathrm{T}} + \boldsymbol{\omega})\mathbf{E}^\infty + (\mathbf{eC}^{-1}\mathbf{h}^{\mathrm{T}} + \boldsymbol{\alpha})\mathbf{H}^\infty + \mathbf{eC}^{-1}\boldsymbol{\sigma}^\infty\right]^{\mathrm{T}} \{-\sin\beta_k, \cos\beta_k\}^{\mathrm{T}}, \\
p_4(\beta_k) &= -\left[(\mathbf{hC}^{-1}\mathbf{e}^{\mathrm{T}} + \boldsymbol{\alpha})\mathbf{E}^\infty + (\mathbf{hC}^{-1}\mathbf{h}^{\mathrm{T}} + \boldsymbol{\gamma})\mathbf{H}^\infty + \mathbf{hC}^{-1}\boldsymbol{\sigma}^\infty\right]^{\mathrm{T}} \{-\sin\beta_k, \cos\beta_k\}^{\mathrm{T}},
\end{aligned}
\tag{17}
$$

where $\boldsymbol{\sigma}^\infty = \{\sigma_{11}^\infty, \sigma_{22}^\infty, \sigma_{12}^\infty\}^{\mathrm{T}}$, $\mathbf{E}^\infty = \{E_1^\infty, E_2^\infty\}^{\mathrm{T}}$, $\mathbf{H}^\infty = \{H_1^\infty, H_2^\infty\}^{\mathrm{T}}$ and $\mathbf{C}$, $\mathbf{e}$, $\mathbf{h}$, $\boldsymbol{\alpha}$, $\boldsymbol{\gamma}$ and $\boldsymbol{\omega}$ are defined in Appendix A for plane strain problems.

The integral Equation (14) together with the constraint Equation (16) are solved by using a numerical integration scheme based on Chebyshev polynomials (Erdogan and Gupta, 1972; Erdogan, 1978). The unknown functions $\rho_j(\xi_k)$ are expressed in terms of Chebyshev polynomials of the first kind, i.e.,

$$
\rho_j(t_k) = \frac{1}{\sqrt{1 - t_k^2}} \sum_{l=0}^{M} v_{jkl}\tau_l(t_k), \tag{18}
$$

where $t_k = \xi_k/a_k$, $(-a_k < \xi_k < a_k)$, $\tau_l(t_k)$ are the Chebyshev polynomials of the first kind, v_{jkl} denotes the coefficients of the Chebyshev polynomial expansion, and M denotes the number of Gauss–Chebyshev collocation points.

After solving the Equation (14), the coupled field at any point in the medium can be obtained. Let $\boldsymbol{\Sigma}_{2s}^k = \left\langle \sigma_{21s}^{(k)}, \sigma_{22s}^{(k)}, D_{2s}^{(k)}, B_{2s}^{(k)} \right\rangle^{\mathrm{T}}$ denotes the singular part of the generalized stress vector of the kth crack which is required in the derivation of field intensity factors. It can be shown that,

$$
\begin{aligned}
\Sigma_{2is}^{(k)} &= 2\mathrm{Re}\sum_{j=1}^{4}\left[F_{ij}(\mu_j, \beta_k)\int_{-a_k}^{a_k} \frac{\rho_j(\xi_k)}{(\eta_k - \xi_k)(\cos\beta_k + \mu_j \sin\beta_k)}\,\mathrm{d}\xi_k\right] \\
&= 2\pi\mathrm{Re}\sum_{j=1}^{4}\left\{[F_{ij}(\mu_j, \beta_k)/(\cos\beta_k + \mu_j \sin\beta_k)]\sum_{l=0}^{M}\left[v_{jkl}\left(t_k - \sqrt{t_k^2 - 1}\right)^l / (t_k^2 - 1)\right]\right\}.
\end{aligned}
\tag{19}
$$

The generalized field intensity vector, $\mathbf{K}^{(k)}$, at a tip of the *kth* crack has four elements: two SIFs, the EDIF and the MIIF. Therefore,

$$\mathbf{K}^{(k)} = \left\langle K_{II}^{(k)}, K_{I}^{(k)}, K_{E}^{(k)}, K_{M}^{(k)} \right\rangle^{\mathrm{T}}, \tag{20a}$$

$$K_i^{(k)} = \lim_{r \to 0} \sqrt{2\pi r} \, \Sigma_{2is}^{(k)}$$

$$= \pm \sqrt{\pi a_k} \left\{ 2\pi \operatorname{Re} \sum_{j=1}^{4} \left[F_{ij}(\mu_j, \beta_k) \frac{\sum\limits_{l=0}^{M} v_{jkl} \tau_l(\pm 1)}{(\cos\beta_k + \mu_j \sin\beta_k)} \right] \right\}, \quad (i = 1, 2, 3, 4), \tag{20b}$$

where r is the distance ahead of a crack tip along the crack line, and the positive and negative signs in the right hand side of Equation (20) correspond to the right and left crack tips, respectively.

The energy release rate can now be calculated by using the crack closure integral (Park and Sun, 1995). For a magnetoelectroelastic solid, the total energy release rate is the sum of the mechanical energy release rate, the electric energy release rate and the magnetic energy release rate. Consider the case of a single crack without loss of any generality and drop the superscript and subscript k from all field variables for convenience. Suppose the crack extend by δ (self-similar), then the total energy release rate (TERR) can be expressed as,

$$G = \lim_{\delta \to 0} \frac{1}{2\delta} \int_0^{\delta} \{\sigma_{i2}(x)\Delta u_i(\delta - x) + D_2(x)\Delta\phi(\delta - x) + B_2(x)\Delta\varphi(\delta - x)\}\mathrm{d}x,$$
$$\text{where } i = 1, 2. \tag{21}$$

The Mode I and Mode II mechanical energy release rates (MERR) are given by,

$$G_I^M = \lim_{\delta \to 0} \frac{1}{2\delta} \int_0^{\delta} \sigma_{22}(x)\Delta u_2(\delta - x)\mathrm{d}x \tag{22a}$$

and

$$G_{II}^M = \lim_{\delta \to 0} \frac{1}{2\delta} \int_0^{\delta} \sigma_{12}(x)\Delta u_1(\delta - x)\mathrm{d}x. \tag{22b}$$

It can be shown that TERR, and Mode I and Mode II MERRs are related to the crack tip SIFs, EDIF and MIIF in the following manner.

$$G = \frac{1}{4}\mathbf{K}^{\mathrm{T}}\mathbf{\Omega}\mathbf{K}, \tag{23a}$$

$$G_I^M = \frac{1}{4}\left[\Omega_{21}K_I K_{II} + \Omega_{22}(K_I)^2 + \Omega_{23}K_I K_E + \Omega_{24}K_I K_M\right] \tag{23b}$$

and

$$G_{II}^M = \frac{1}{4}\left[\Omega_{11}(K_{II})^2 + \Omega_{12}K_I K_{II} + \Omega_{13}K_{II} K_E + \Omega_{14}K_{II} K_M\right], \tag{23c}$$

where $\mathbf{\Omega} = 2\operatorname{Re}(i\mathbf{A}\mathbf{L}^{-1})$.

The above relations clearly show that the total energy release rate and the Mode I and Mode II mechanical energy release rates for plane problems depend on all four field intensity factors.

4. J_i-Integral and M-integral analysis

4.1. SINGLE CRACK CASE

Path-independent J_i-integrals ($i = 1, 2$) and M-integral for a single crack in an elastic material were originally defined by Rice (1968), Knowles and Sternberg (1972) and Budiansky and Rice (1973). Later, Suo et al. (1992) and Pak (1992) showed that for a piezoelectric medium,

$$J_1 = \oint_C \left[\frac{1}{2} \left(\sigma_{ij} \varepsilon_{ij} - D_i E_i \right) dx_2 - n_i \sigma_{ip} u_{p,1} ds - n_i D_i \phi_{,1} ds \right], \tag{24a}$$

$$J_2 = \oint_C \left[-\frac{1}{2} \left(\sigma_{ij} \varepsilon_{ij} - D_i E_i \right) dx_1 - n_i \sigma_{ip} u_{p,2} ds - n_i D_i \phi_{,2} ds \right], \tag{24b}$$

$$M = \oint_C \left[\frac{1}{2} (\sigma_{ij} \varepsilon_{ij} - D_i E_i) x_l n_l - n_i \sigma_{ip} u_{p,l} x_l - n_i D_i \phi_{,l} x_l \right] ds, \tag{24c}$$

where $i, j, p, l = 1, 2$; C denotes a closed contour around a crack; and n_l is the outward unit normal to C.

In the present paper, the authors extend the J_i- and M-integrals to magnetoelectroelastic solids and obtain the following results.

$$J_1 = \oint_C \left[\frac{1}{2} \left(\sigma_{ij} \varepsilon_{ij} - D_i E_i - B_i H_i \right) dx_2 - n_i \sigma_{ip} u_{p,1} ds - n_i D_i \phi_{,1} ds - n_i B_i \varphi_{,1} ds \right], \tag{25a}$$

$$J_2 = \oint_C \left[-\frac{1}{2} \left(\sigma_{ij} \varepsilon_{ij} - D_i E_i - B_i H_i \right) dx_1 - n_i \sigma_{ip} u_{p,2} ds - n_i D_i \phi_{,2} ds - n_i B_i \varphi_{,2} ds \right], \tag{25b}$$

$$M = \oint_C \left[\frac{1}{2} (\sigma_{ij} \varepsilon_{ij} - D_i E_i - B_i H_i) x_l n_l - n_i \sigma_{ip} u_{p,l} x_l - n_i D_i \phi_{,l} x_l - n_i B_i \varphi_{,l} x_l \right] ds. \tag{25c}$$

In the following, the dependence of the J_i and M-integrals on the coordinate system is examined which is useful to the extension of the J_i and M-integrals to the multiple cracks case. Consider a new Cartesian coordinate system (x_1^*, x_2^*) and the J_i and M-integrals can be expressed with respect to the new system of coordinates as,

$$J_1^* = \oint_C \left[\frac{1}{2} (\sigma_{ij}^* \varepsilon_{ij}^* - D_i^* E_i^* - B_i^* H_i^*) dx_2^* - n_i^* \sigma_{ip}^* u_{p,1}^* ds - n_i^* D_i^* \phi_{,1}^* ds - n_i^* B_i^* \varphi_{,1}^* ds \right] \tag{26a}$$

$$J_2^* = \oint_C \left[-\frac{1}{2} (\sigma_{ij}^* \varepsilon_{ij}^* - D_i^* E_i^* - B_i^* H_i^*) dx_1^* - n_i^* \sigma_{ip}^* u_{p,2}^* ds - n_i^* D_i^* \phi_{,2}^* ds - n_i^* B_i^* \varphi_{,2}^* ds \right] \tag{26b}$$

$$M^* = \oint_C \left[\frac{1}{2} (\sigma_{ij}^* \varepsilon_{ij}^* - D_i^* E_i^* - B_i^* H_i^*) x_l^* n_l^* - n_i^* \sigma_{ip}^* u_{p,l}^* x_l^* - n_i^* D_i^* \phi_{,l}^* x_l^* - n_i^* B_i^* \varphi_{,l}^* x_l^* \right] ds \tag{26c}$$

Assume that the coordinate system (x_1^*, x_2^*) is obtained from a simple rotation of the coordinate system (x_1, x_2) by angle β. Following relationships can be established by using the rules for coordinate transformation of the first and second order tensors.

$$x_l n_l = x_l^* n_l^*, \qquad n_i \sigma_{ip} u_{p,l} x_l = n_i^* \sigma_{ip}^* u_{p,l}^* x_l^*,$$
$$n_i D_i \phi_{,l} x_l = n_i^* D_i^* \phi_{,l}^* x_l^*, \qquad n_i B_i \varphi_{,l} x_l = n_i^* B_i^* \varphi_{,l}^* x_l^* \qquad (27)$$

and

$$\sigma_{ij} \varepsilon_{ij} - D_i E_i - B_i H_i = \sigma_{ij}^* \varepsilon_{ij}^* - D_i^* E_i^* - B_i^* H_i^*. \qquad (28)$$

It can be shown by using Equations (26)–(28) and (25) that,

$$J_1 = J_1^* \cos \beta - J_2^* \sin \beta, \qquad J_2 = J_1^* \sin \beta + J_2^* \cos \beta, \quad M = M^* \qquad (29)$$

Equation (29) reveals that J_i-integrals $(i = 1, 2)$ change when the coordinate system is rotated whereas the M-integral is unchanged. Now assume that the coordinate systems (x_1, x_2) and (x_1^*, x_2^*) are related by a pure translation (zero rotation) such that,

$$x_1 = x_1^* + \Delta x_1, \qquad x_2 = x_2^* + \Delta x_2. \qquad (30)$$

According to Equations (25), (26) and (30),

$$J_1 = J_1^*, \quad J_2 = J_2^*, \quad M = M^* + \Delta x_1 J_1 + \Delta x_2 J_2 \qquad (31)$$

Equation (31) shows that the J_i-integrals are independent of the translation of the coordinate system whereas the M-integral is not.

4.2. MULTI-CRACKS CASE

Consider the system shown in Figure 2. In order to evaluate the J_i and M-integrals for a set of cracks, the closed contours Γ and Γ_k are used. The contour Γ encloses all cracks, while the contour Γ_k encloses only the kth crack. All integrals are evaluated with respect to the global coordinate system (x_1, x_2). According to the path-independent nature of the J_i and M-integrals, it can be shown that (Chen, 2001a),

$$J_1 = \sum_{k=1}^{N} J_{1k}, \qquad J_2 = \sum_{k=1}^{N} J_{2k}, \qquad M = \sum_{k=1}^{N} M_k, \qquad (32)$$

where J_1, J_2 and M are defined by Equation (25) using the contour Γ enclosing all cracks whereas J_{1k}, J_{2k} and M_k are defined by Equation (25) with the contour Γ_k associated with the kth crack.

In view of Equations (29) and (31), the J_i and M-integrals defined with respect to the global coordinate system can be expressed in terms of the integrals $J_{1k}^{(k)}$, $J_{2k}^{(k)}$ and $M_k^{(k)}$ based on the local coordinate system (x_1^k, x_2^k) and contour Γ_k. Following relationships are obtained.

$$J_1 = \sum_{k=1}^{N} J_{1k} = \sum_{k=1}^{N} \left[J_{1k}^{(k)} \cos \beta_k - J_{2k}^{(k)} \sin \beta_k \right], \tag{33a}$$

$$J_2 = \sum_{k=1}^{N} J_{2k} = \sum_{k=1}^{N} \left[J_{1k}^{(k)} \sin \beta_k + J_{2k}^{(k)} \cos \beta_k \right], \tag{33b}$$

$$M = \sum_{k=1}^{N} M_k = \sum_{k=1}^{N} \left[M_k^{(k)} + x_{01}^k J_{1k} + x_{02}^k J_{2k} \right] \tag{33c}$$

and $J_{1k}^{(k)}$, $J_{2k}^{(k)}$ and $M_k^{(k)}$ can be expressed in terms of field intensity factors as (Suo et al., 1992),

$$J_{1k}^k = \tfrac{1}{4}(\mathbf{K}^{(k)R})^{\mathrm{T}} \boldsymbol{\Omega} \mathbf{K}^{(k)R} - \tfrac{1}{4}(\mathbf{K}^{(k)L})^{\mathrm{T}} \boldsymbol{\Omega} \mathbf{K}^{(k)L}, \tag{34a}$$

$$J_{2k}^k = \tfrac{1}{4}(\mathbf{K}^{(k)R})^{\mathrm{T}} \boldsymbol{\Theta}\boldsymbol{\Omega} K^{(k)R} - \tfrac{1}{4}(\mathbf{K}^{(k)L})^{\mathrm{T}} \boldsymbol{\Theta}\boldsymbol{\Omega} K^{(k)L} + \int_{-a_k}^{a_k} (W^+ - W^-) \mathrm{d}x_1^k, \tag{34b}$$

$$M_k^{(k)} = \left(\tfrac{1}{4} \left(\mathbf{K}^{(k)R} \right)^{\mathrm{T}} \boldsymbol{\Omega} \mathbf{K}^{(k)R} + \tfrac{1}{4} \left(\mathbf{K}^{(k)L} \right)^{\mathrm{T}} \boldsymbol{\Omega} \mathbf{K}^{(k)L} \right) a_k, \tag{34c}$$

where W^+ and W^- denote the magnetoelectroelastic energy density W on the upper and lower crack faces, respectively; superscripts R and L denote the right and left crack tips respectively, and

$$\boldsymbol{\Theta} = -\mathrm{Re}(\Delta \mathbf{L}^{-1}), \tag{35a}$$

$$\boldsymbol{\Delta} = [-\mu_1 \mathbf{b}_1, -\mu_2 \mathbf{b}_2, -\mu_3 \mathbf{b}_3, -\mu_4 \mathbf{b}_4]. \tag{35b}$$

Equations (33) and (34) present the relationship between the J_i and M integrals and the field intensity factors for a cluster of arbitrarily oriented cracks.

4.3. Proof of the conservation law of the J_i-integrals

Chen (2001b) proved that for a piezoelectric material subjected to remote uniform loading,

$$J_1 = \sum_{k=1}^{N} J_{1k} = 0, \qquad J_2 = \sum_{k=1}^{N} J_{2k} = 0. \tag{36}$$

It can be easily proven that the above identity is also true for magnetoelectroelastic materials. Consider a closed rectangular far-field contour Γ_∞ (*abcd*) encompassing all cracks (Figure 2). According to the path-independent nature of the *J*-integral, the solutions along contours Γ and Γ_∞ should be identical. Therefore,

$$J_1 = \oint_{\Gamma_\infty} \left[\frac{1}{2} \left(\sigma_{ij}^\infty \varepsilon_{ij}^\infty - D_i^\infty E_i^\infty - B_i^\infty H_i^\infty \right) \mathrm{d}x_2 - n_i \sigma_{ip}^\infty u_{p,1}^\infty \mathrm{d}s - n_i D_i^\infty \phi_{,1}^\infty \mathrm{d}s - n_i B_i^\infty \varphi_{,1}^\infty \mathrm{d}s \right] \tag{37a}$$

$$J_2 = \oint_{\Gamma_\infty} \left[-\frac{1}{2} \left(\sigma_{ij}^\infty \varepsilon_{ij}^\infty - D_i^\infty E_i^\infty - B_i^\infty H_i^\infty \right) \mathrm{d}x_1 - n_i \sigma_{ip}^\infty u_{p,2}^\infty \mathrm{d}s - n_i D_i^\infty \phi_{,2}^\infty \mathrm{d}s - n_i B_i^\infty \varphi_{,2}^\infty \mathrm{d}s \right] \tag{37b}$$

Note that $dx_1 = 0$ on $\overline{ab}$ and $\overline{cd}$, and $dx_2 = 0$ on $\overline{da}$ and $\overline{bc}$. Equation (37) can be rewritten as,

$$J_1 = \frac{1}{2}\sigma_{ij}^\infty \varepsilon_{ij}^\infty \left(\int_a^b dx_2 - \int_d^c dx_2\right) - \frac{1}{2}D_i^\infty E_i^\infty \left(\int_a^b dx_2 - \int_d^c dx_2\right) - \frac{1}{2}B_i^\infty H_i^\infty \left(\int_a^a dx_2 - \int_d^c dx_2\right)$$
$$+\sigma_{1p}^\infty \left(\int_d^c u_{p,1}^\infty dx_2 - \int_a^b u_{p,1}^\infty dx_2\right) + D_1^\infty \left(\int_d^c \phi_{,1}^\infty dx_2 - \int_a^b \phi_{,1}^\infty dx_2\right) + B_1^\infty \left(\int_d^c \varphi_{,1}^\infty dx_2 - \int_a^b \varphi_{,1}^\infty dx_2\right)$$
$$+\sigma_{2p}^\infty \left(\int_b^c u_{p,1}^\infty dx_1 - \int_a^d u_{p,1}^\infty dx_1\right) + D_2^\infty \left(\int_b^c \phi_{,1}^\infty dx_1 - \int_a^d \phi_{,1}^\infty dx_1\right) + B_2^\infty \left(\int_b^c \varphi_{,1}^\infty dx_1 - \int_a^d \varphi_{,1}^\infty dx_1\right),$$

(38a)

$$J_2 = -\frac{1}{2}\sigma_{ij}^\infty \varepsilon_{ij}^\infty \left(\int_b^c dx_1 - \int_a^d dx_1\right) - \frac{1}{2}D_i^\infty E_i^\infty \left(\int_b^c dx_1 - \int_a^d dx_1\right) - \frac{1}{2}B_i^\infty H_i^\infty \left(\int_b^c dx_1 - \int_a^d dx_1\right)$$
$$+\sigma_{1p}^\infty \left(\int_d^c u_{p,2}^\infty dx_2 - \int_a^b u_{p,2}^\infty dx_2\right) + D_1^\infty \left(\int_d^c \phi_{,2}^\infty dx_2 - \int_a^b \phi_{,2}^\infty dx_2\right) + B_1^\infty \left(\int_d^c \varphi_{,2}^\infty dx_2 - \int_a^b \varphi_{,2}^\infty dx_2\right)$$
$$+\sigma_{2p}^\infty \left(\int_b^c u_{p,2}^\infty dx_1 - \int_a^d u_{p,2}^\infty dx_1\right) + D_2^\infty \left(\int_b^c \phi_{,2}^\infty dx_1 - \int_a^d \phi_{,2}^\infty dx_1\right) + B_2^\infty \left(\int_b^c \varphi_{,2}^\infty dx_1 - \int_a^d \varphi_{,2}^\infty dx_1\right).$$

(38b)

It can be easily seen that the first three terms on the right-hand side of Eqs. (38a) and (38b) vanish because $\left(\int_a^b dx_2 - \int_d^c dx_2\right) = 0$ and $\left(\int_b^c dx_1 - \int_a^d dx_1\right) = 0$. Likewise, the fourth to the ninth terms on the right side of the equations also vanish because of the uniform remote loading field. Equation (36) therefore holds true for magneto-electroelastic materials. The conversation law of the J_i-integrals is helpful in checking the accuracy of numerical results for multiple cracks problems.

5. Numerical results and discussion

Selected numerical results are presented in this section to investigate the fracture behaviour of a magnetoelectroelastic composite, namely $BaTiO_3$–$CoFe_2O_4$. Its piezoelectric phase is $BaTiO_3$, while its piezomagnetic phase is $CoFe_2O_4$. The volume fraction of $BaTiO_3$ is 50%. The material constants of $BaTiO_3$–$CoFe_2O_4$ composite are: $C_{11} = 226\,GPa$, $C_{12} = 124\,GPa$, $C_{22} = 216\,GPa$, $C_{66} = 44\,GPa$, $e_{21} = -2.2\,C/m^2$, $e_{22} = 9.3\,C/m^2$, $e_{16} = 5.8\,C/m^2$, $\omega_{11} = 56.4 \times 10^{-10}\,C^2/Nm^2$, $\omega_{22} = 63.5 \times 10^{-10}\,C^2/Nm^2$, $h_{21} = 290.2\,N/Am$, $h_{22} = 350\,N/Am$, $h_{16} = 275\,N/Am$, $\gamma_{11} = 297 \times 10^{-6}\,Ns^2/C^2$, $\gamma_{22} = 83.5 \times 10^{-6}\,Ns^2/C^2$, $\alpha_{11} = 5.367 \times 10^{-12}\,Ns/VC$, $\alpha_{22} = 2737.5 \times 10^{-12}\,Ns/VC$ (Li, 2000; Song and Sih, 2003). Plane strain condition is assumed in the analysis and the remote mechanical loading for all cases considered in the numerical study is given by $\sigma_{12}^\infty = 0$, $\sigma_{11}^\infty = 0$, $\sigma_{22}^\infty = 0.6\,MPa$. The focus of the numerical study is to examine the dependence of fracture behaviour on electric and magnetic loading. The mechanical loading is therefore not changed. Electric and magnetic loading magnitudes are relatively small to ensure linear behaviour and are kept well below the fields required for polarization switching.

5.1. SINGLE CRACK CASE

Consider the single impermeable crack shown in Figure 3. The infinite plane is subjected to electric and magnetic fields in the x_2 direction in addition to remote tension
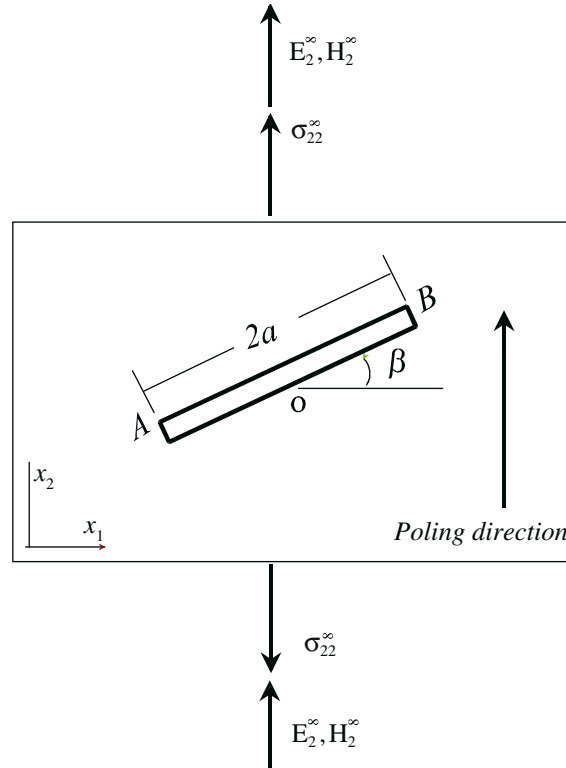
Figure 3. Geometry of an arbitrarily oriented single crack and remote loading system.

in the same direction. The half-length and orientation of the crack with respect to the x_1 direction are denoted by a and β, respectively. Figure 4 shows the M-integral, the total energy release rate G_A and the mechanical strain energy release rate G_A^M at the crack tip A for $\beta = 0°$, 30° and 45°. Note that G_A and G_A^M are normalized by G_0 and G_0^M, respectively, where G_0 and G_0^M denote the total energy release rate and the mechanical energy release rate of an identical horizontal crack ($\beta = 0°$) under pure tension in the x_2 direction.

It is clear from Figure 4 that the M-integral and the total strain energy release rate show similar effects of applied electric and magnetic loading. For example, both M and G are decreased by an increasing applied electric or magnetic loading except in the case of a very weak positive electric field ($0 < E_2^\infty < 0.4$ KV/m) and a very weak positive magnetic field ($0 < H_2^\infty < 0.006$ KA/m). This implies that both electric and magnetic fields generally inhibit the propagation of an impermeable crack. As can be seen from Figure 4, M and G curves are not symmetric about the zero electric/magnetic loading point. The slopes of M and G curves for a negative electric/magnetic field are slightly higher when compared to a positive electric/magnetic field. A horizontal crack shows higher M and G values when compared to inclined cracks, which implies that a horizontal impermeable crack is less stable than an inclined crack. The dependence of magnitude of M and G on crack orientation is substantial. From a physical point of view the limiting case of $\beta = 90°$ should be the most stable configuration under the applied loading shown in Figure 3.
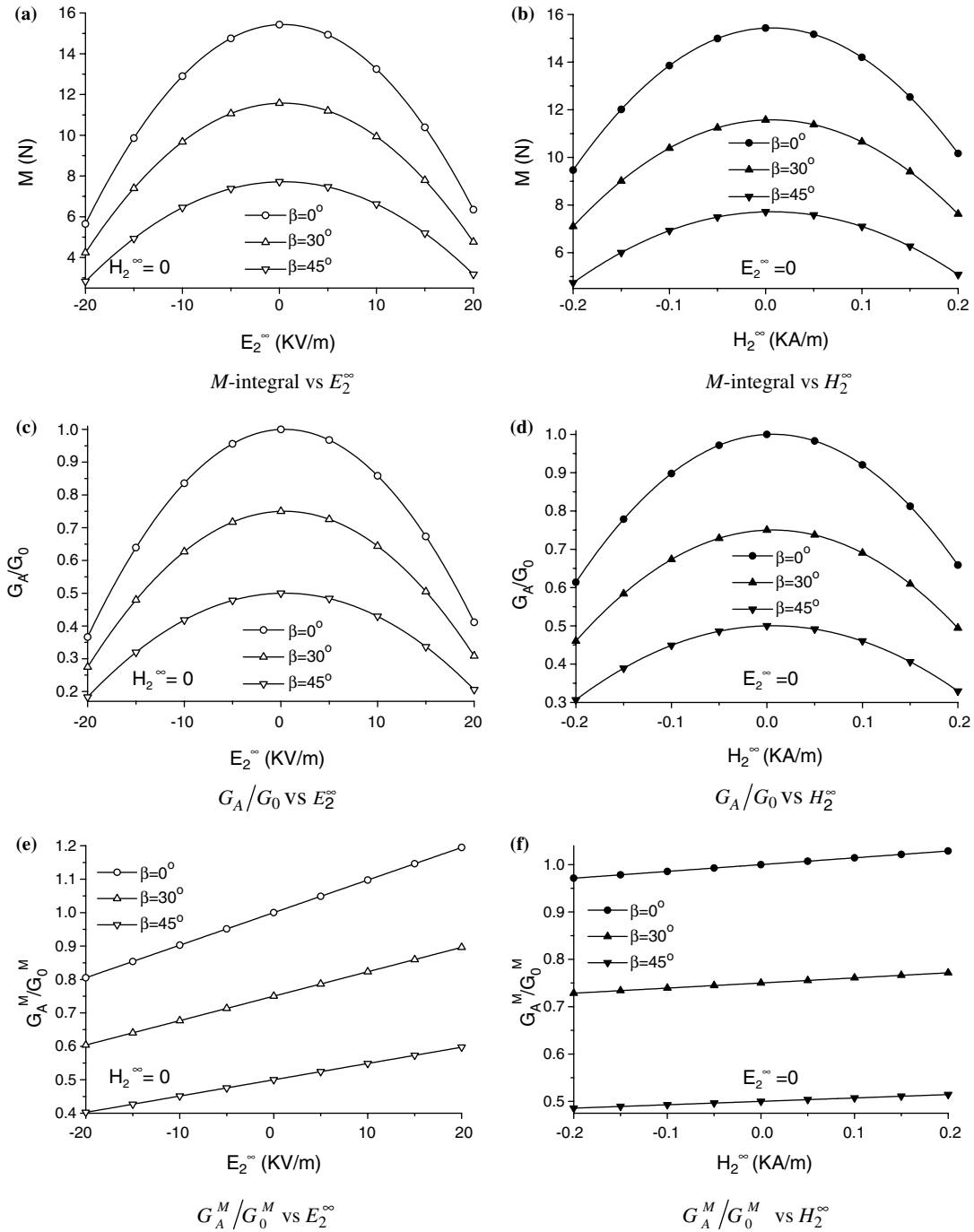
(a) M-integral vs E_2^∞

(b) M-integral vs H_2^∞

(c) G_A/G_0 vs E_2^∞

(d) G_A/G_0 vs H_2^∞

(e) G_A^M/G_0^M vs E_2^∞

(f) G_A^M/G_0^M vs H_2^∞

Figure 4. Variation of M-integral, G_A/G_0 and G_A^M/G_0^M with applied electric field and magnetic field.

The mechanical strain energy release rate, G_A^M/G_0^M, shows substantially different dependence on applied electric and magnetic fields when compared to the dependence of M-integral and total energy release rate on electric and magnetic loading. Mechanical energy release rate increases with increasing positive electric field and
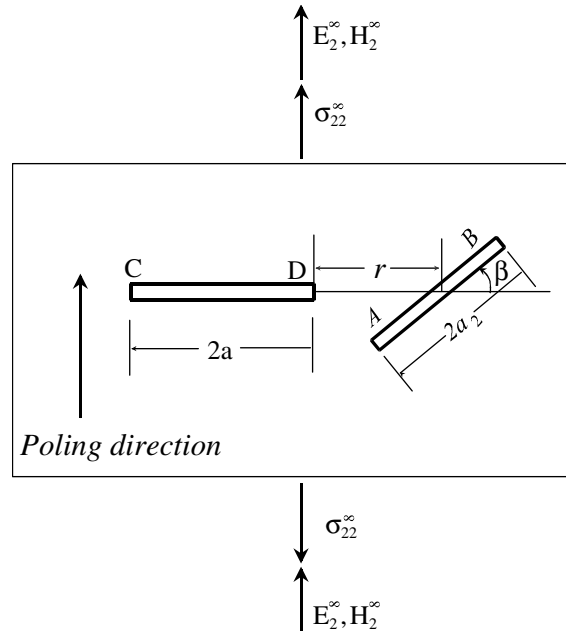
Figure 5. Geometry of two cracks case and remote loading.

decreases with increasing negative electric fields. This implies that a positive electric field promotes crack propagation, while a negative electric field inhibits it. Mechanical energy release rate shows negligible dependence on applied magnetic field. This behaviour is also very different from strong dependence of M and G on magnetic field observed from Figure 4. Mechanical energy release rate also shows substantial dependence on crack orientation. Although Park and Sun (1995) argued that fracture is a mechanical process and mechanical energy release rate show better agreement with their experiments, there is no fundamental reason to consider only mechanical energy. The authors are not aware of any experimental results to do a qualitative comparison with the numerical results shown in Figure 4. However, given that G and M show similar behaviour and there is no strong theoretical basis for the mechanical energy release rate, it appears that the use of G_A^M as a fracture parameter for magnetoelectroelastic materials is questionable.

5.2. Interaction between two cracks

Figure 5 shows an infinite plane with two cracks (*AB* and *CD*) subjected to remote loading. The lengths of the cracks are denoted by $2a$ and $2a_2$. In problems involving more than one crack, the behaviour of cracks is controlled by several geometric parameters (e.g. length ratio, distance between the cracks and relative crack orientation) and some of these parameters obviously have to be fixed in a parametric study. The crack *CD* is assumed to be a horizontal crack, while the centre of crack *AB* is placed along the line *CD* at a distance 'r' from D and has orientation angle β. In the numerical study, the behaviour of the system is studied for the case $a_2 = a$, $r = 1.1a$ and $0° \leq \beta \leq 180°$.

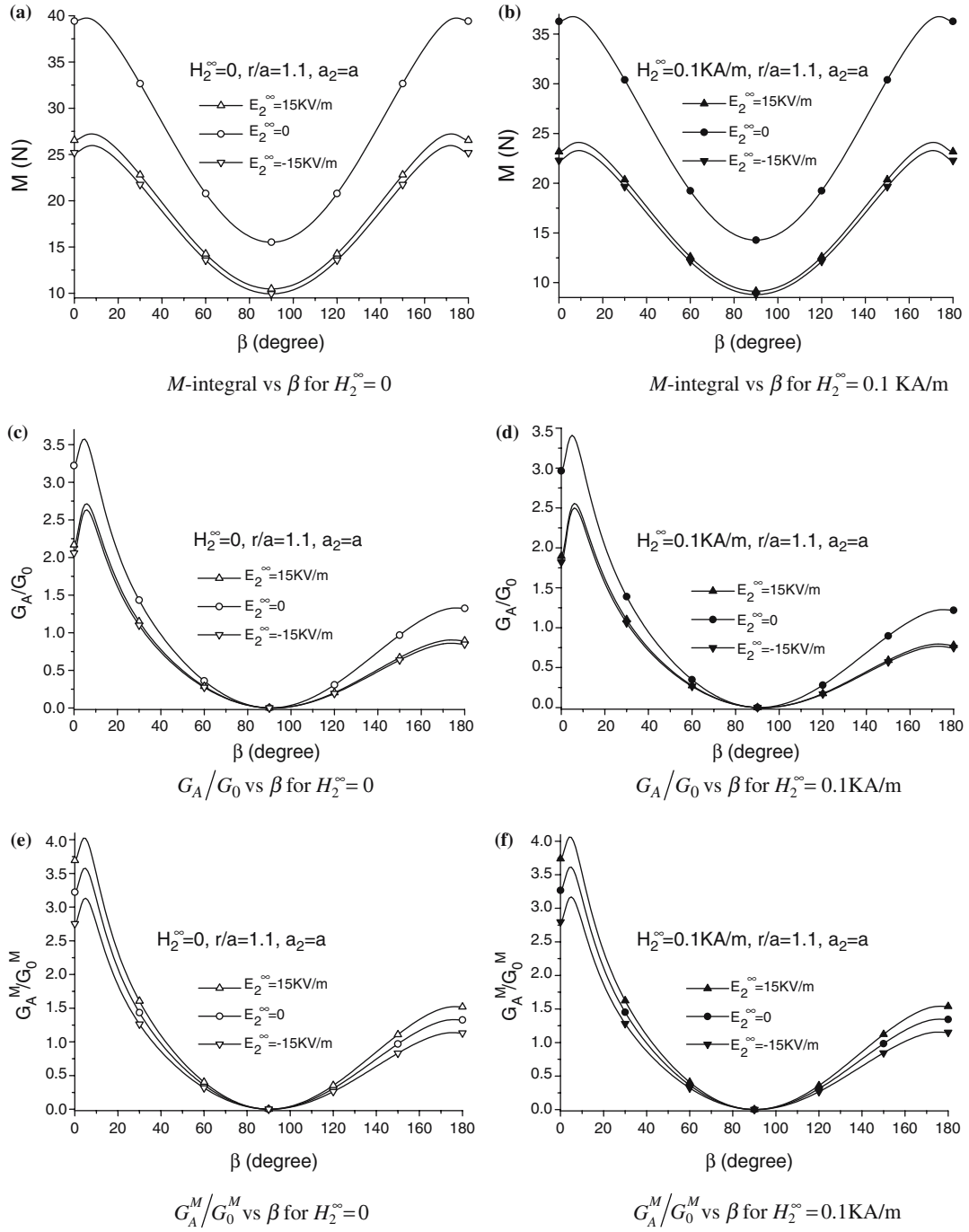Figure 6. Variation of *M*-integral, G_A/G_0 and G_A^M/G_0^M with orientation angle β for two cracks.

The *M*-integral and the total energy release rate and the mechanical strain energy release rate corresponding to tip *A* are shown in Figure 6 for different values of crack orientation angle β.

It is noted that both positive and negative electric fields reduce the magnitude of *M* and the presence of a positive remote magnetic field in addition to remote tension

further reduces the magnitude of M. An electric field or a magnetic field therefore inhibits crack propagation in the case of two cracks. This behaviour is similar to that noted earlier for a single crack (see Figure 4). Figures 6a and b show that M–integral has its highest value when the cracks are nearly colinear while the lowest magnitude of M (most stable configuration of crack AB) occurs when the two cracks are perpendicular to each other. Furthermore, the profiles of M-integral are symmetric about $\beta = 90°$. The above features of M-integral are consistent with the physical behaviour of the system shown in Figure 5. Figures 6c–6f show the total energy release rate and the mechanical strain energy release rate at the crack tip A. The minimum values of the energy release rates correspond to $\beta = 90°$ similar to the M-integral but the magnitude is zero. The values of G_A/G_0 or G_A^M/G_0^M for $\beta = 0°$ and $180°$ are obviously not equal for this case as the energy release rates at crack tip A is not symmetric about $\beta = 90°$. As the crack AB is rotated, the most unstable position of AB corresponds to $\beta \approx 8°$ (consistent with the M-integral) and both total and mechanical energy release rates thereafter decreases with increasing β (crack tip A moves away from tip D) reaching the most stable configuration when $\beta = 90°$. For $\beta > 90°$, both G and M increases with increasing β. Energy release rates show less dependence on the applied electric field when compared to the M-integral and the mechanical energy release rate is slightly increased by a positive electric field. The influence of magnetic field is also lesser in the case of mechanical energy release rate.

Figure 7 shows the variation of mechanical strain energy release rate and the total energy release rate at crack tip D with the orientation angle β of crack AB, and magnitudes of applied electric field and applied magnetic field. It is noted from Figure 7 that the variation of the total energy release rate of crack CD is similar to the variation of the M-integral Figure 6. The curves have their minimum value at and are symmetric about $\beta = 90°$. Furthermore, the variation of mechanical energy release rate at D with β is also similar to that observed in Figure 6 for the M-integral but the dependence of G_D^M/G_0^M on electric field is different. The orientation angle of crack AB has a significant effect on the energy release rates of crack CD and the maximum influence of AB occurs when the two cracks are not co-linear and this is consistent with the behaviour of M-integral in Figure 6. Based on the results shown in Figures 4, 6 and 7, it is clear that the mechanical energy release rate predicts different fracture behaviour under electric and magnetic loading. On the other hand, the total energy release rate shows physically reasonable results that closely match the M-integral behaviour for a single crack and horizontally placed crack of a double-crack system (Figure 5). It should be noted that when crack CD is allowed to rotate, the solutions for G_D/G_0 show more complex dependence on β. According to equation (33c), M-integral can be considered as a global measure of damage due to a cluster of cracks whereas energy release rates (total or mechanical) are fracture parameters associated with a tip of one crack. As such energy release rates cannot serve as an overall measure of fracture behaviour of a system of cracks.

In order to check accuracy of the numerical results for the double crack case shown in Figure 5, the conservation law of the J-integral given by Equation (36) is applied. Figure 8 shows $J_{ij}/J_0 (i, j = 1, 2)$, where J_0 is the J-integral of a single horizontal crack under identical remote loading. It can be easily seen from Figure 8 that the conservation law of the J-integrals is satisfied and high accuracy of present numerical solutions is confirmed.
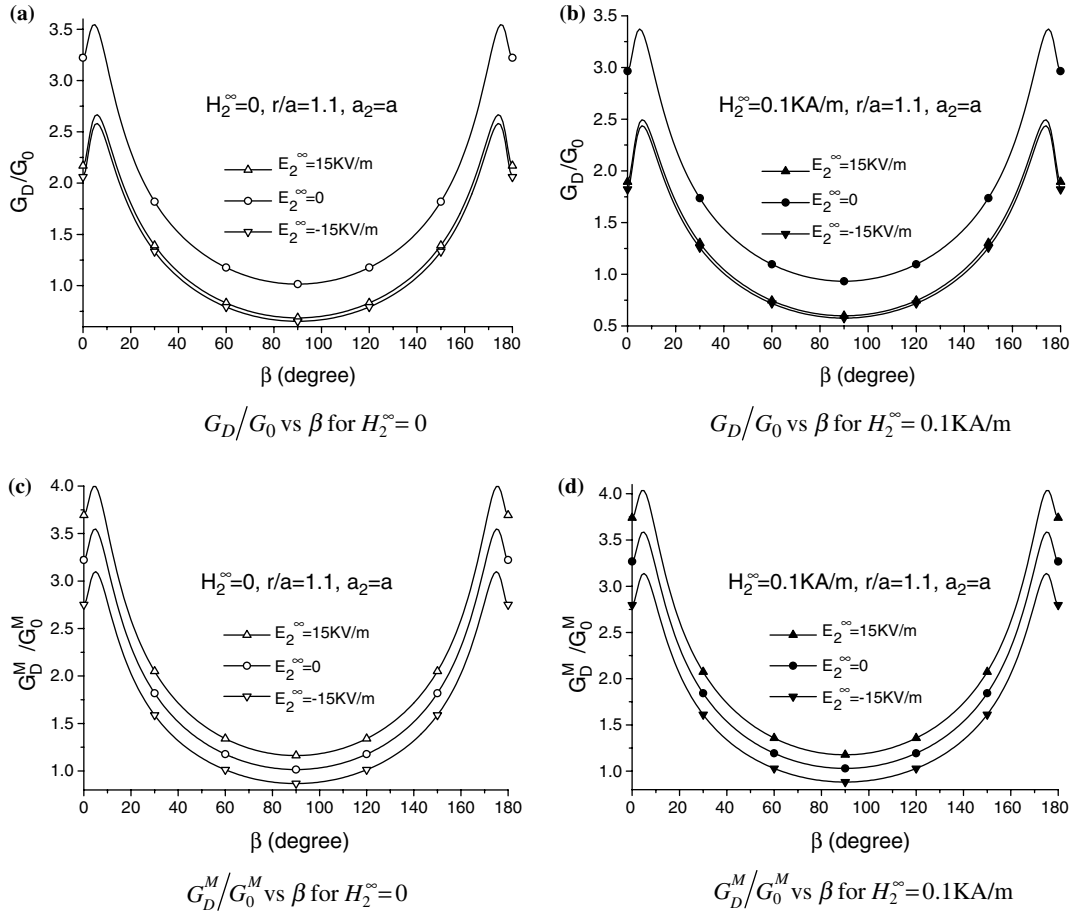
G_D/G_0 vs β for $H_2^\infty = 0$ G_D/G_0 vs β for $H_2^\infty = 0.1$KA/m

G_D^M/G_0^M vs β for $H_2^\infty = 0$ G_D^M/G_0^M vs β for $H_2^\infty = 0.1$KA/m

Figure 7. Variation of G_D/G_0 and G_D^M/G_0^M with orientation angle β for two-crack case.

J_{11}/J_0 and J_{12}/J_0 J_{21}/J_0 and J_{22}/J_0
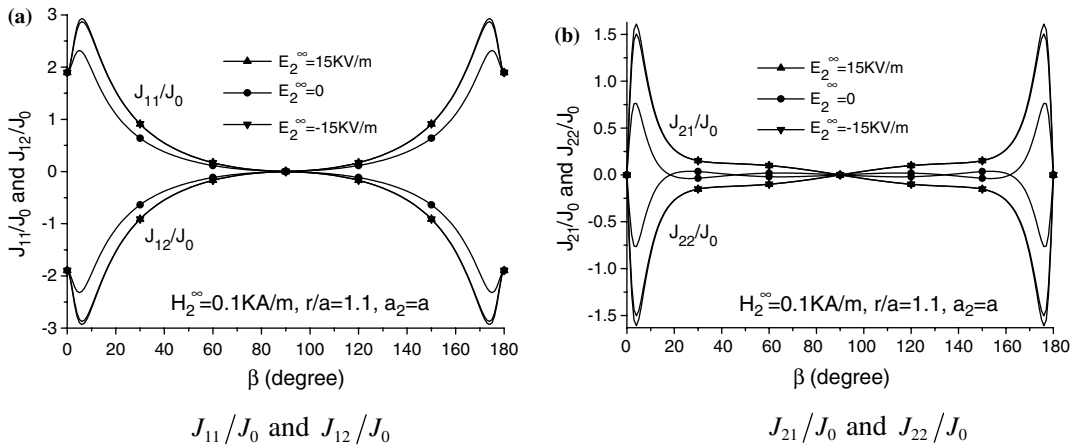
Figure 8. Variation of J-integrals with orientation angle β for two-crack case.
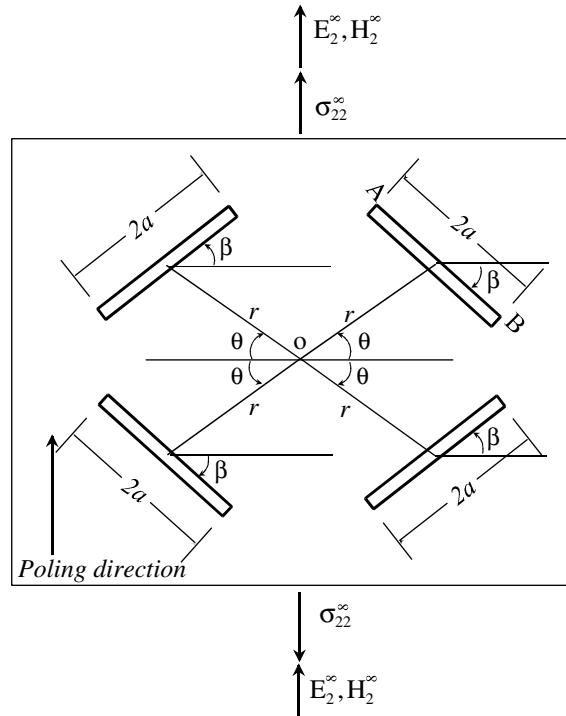
Figure 9. Geometry of four cracks cluster and remote loading.

5.3. CLUSTER OF FOUR CRACKS

A case involving multiple cracks is considered to further demonstrate the application of the *M*-integral in damage assessment of magnetoelectroelastic materials. The system considered is shown in Figure 9 where an infinite plane containing four cracks of identical length $2a$ is subjected to remote tension and magnetic and electric fields in the x_2 direction. The four cracks are symmetrically placed to reduce the total number geometric parameters governing the behaviour of the system. Numerical results are presented for the case $r/a = 1.5$, $\theta = 45°$ and β is changed over the range 0°–180°. The *M*-integral and the total and mechanical strain energy release rates at the crack tip *A* are shown in Figure 10.

It is evident from Figure 10 that the *M*-integral shows physically more realistic behaviour with the minimum value of *M* corresponding to $\beta = 90°$, maximum values for $\beta = 0°$ and 180° and symmetry about $\beta = 90°$. For example, when $\beta = 90°$, all four cracks are parallel to the loading direction and the minimum effect of damage in the medium should be noted as demonstrated by the lowest value of $M(=0)$ in Figure 10. On the other hand, for $\beta = 0°$ and 180°, all cracks are normal to the loading and the maximum effect of damage is felt as characterized by the maximum value of *M*. It is therefore reasonable to assume that *M*-integral represents a reasonable qualitative measure of damage and could be implicitly related to the effective elastic moduli of a solid with microcracks. The dependence of *M* on electric field and magnetic field is similar to that observed previously for single and double crack cases. On the other hand, the numerical results for fracture parameters associated
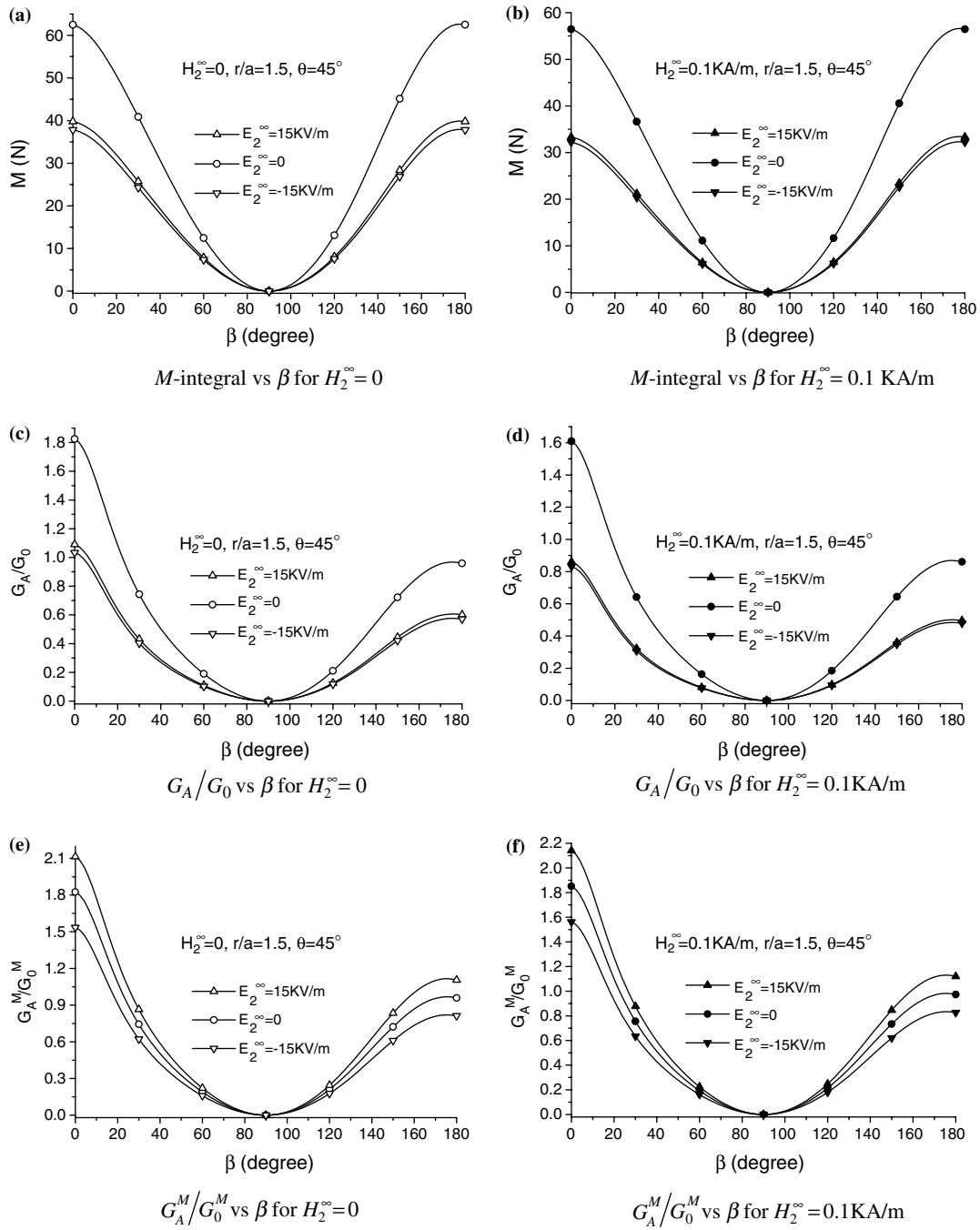
(a) *M*-integral vs β for $H_2^\infty = 0$

(b) *M*-integral vs β for $H_2^\infty = 0.1$ KA/m

(c) G_A / G_0 vs β for $H_2^\infty = 0$

(d) G_A / G_0 vs β for $H_2^\infty = 0.1$ KA/m

(e) G_A^M / G_0^M vs β for $H_2^\infty = 0$

(f) G_A^M / G_0^M vs β for $H_2^\infty = 0.1$ KA/m

Figure 10. Variation of *M*-integral, G_A/G_0 and G_A^M/G_0^M with β for multi-cracks case.

with a single crack tip, such as G_A/G_0 and G_A^M/G_0^M, shown in Figures 10c–10f obviously have different values for $\beta = 0°$ and $180°$ and do not posses symmetry about $\beta = 90°$. Both total and mechanical energy release rates are zero for $\beta = 90°$ (similar to *M*-integral) but it is difficult to obtain a qualitative relationship between damage and energy release rates or to implicitly relate energy release rates to effective elastic
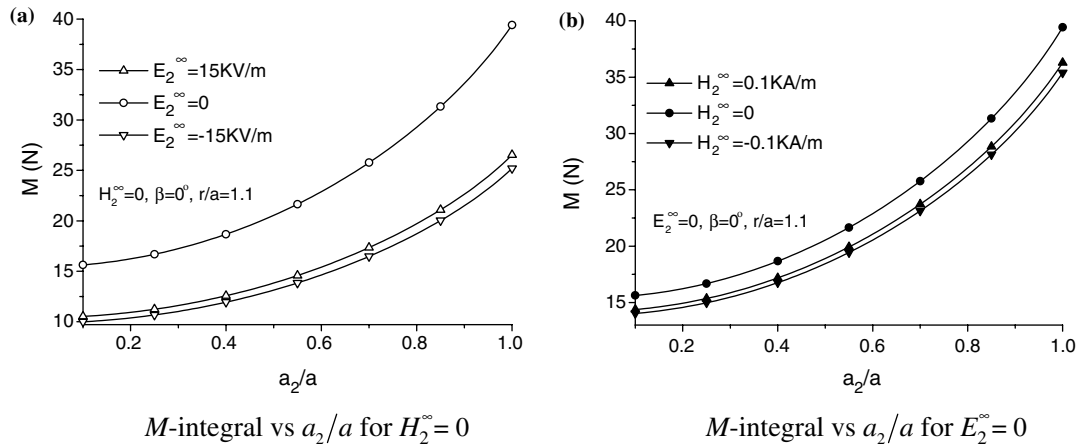
Figure 11. Variation of *M*-integral with a_2/a for a two-crack system with a slowly growing crack.

moduli. The results shown in Figures 4, 6 and 10 confirms that *M*-integral is a better and physically more consistent measure of damage associated with cracks when compared to crack tip based fracture parameters. Certain symmetries associated with physical systems are directly reflected in the *M*-integral solutions whereas crack tip parameters obviously do not show such behaviour for multiple-crack cases. It should be noted that experimental studies are required to identify a suitable fracture criterion for the present class of materials. Unfortunately, such experimental results are not available to validate the adequacy of the three fracture parameters considered in the present study. Nevertheless, theoretical studies are useful in identifying the trends and dependence of fracture parameters and in identifying suitable fracture parameters for experimental validation.

5.4. GROWING CRACK CASE

The merit of the *M*-integral in evaluating damage due to a slowly growing (quasistatic) crack is demonstrated in this section. Consider the system shown in Figure 5 and assume that the crack *AB* is a slowly growing crack characterized by increasing values of a_2/a. Figure 11 shows the variation of the *M*-integral for $0.1 \leq a_2/a \leq 1.0$ for $\beta = 0°$ under different remote electric and magnetic field intensities.

As can be seen from Figure 11, the smallest magnitude of the *M*-integral corresponds to $a_2/a = 0$ and the presence of a second crack increases *M* under both electric and magnetic loading. *M* increases nonlinearly with a_2/a and the slope of M also increases rapidly with increasing length of the second crack. For example, when the length of the growing crack is below 50% of the stationary crack, the increase of *M* is less than 30%. However, the value of *M* nearly doubles as the length increases from *0.5a* to *a*. This behaviour implies that microcracks exceeding a certain critical length could cause brittle failure of a magnetoelectroelastic material under electromagnetic loading. As the second crack grows the damage of the medium increases as reflected by increasing values of *M* and as in the four-crack case the *M*-integral behaviour can be implicitly linked to the reduction of effective elastic modulus of the medium. Figure 11 shows that the presence of an electric field reduces the magnitude of *M* but

the slope of M is not significantly influenced. Similar behaviour is observed when the medium is subjected to a magnetic field.

6. Conclusions

It is shown that the continuously distributed dislocation method originally proposed for elastic materials can be extended to solve crack problems in weakly magnetizable magnetoelectroelastic materials in the absence of hysteresis and spin-ordering effects. The solution for a set of multiple cracks can be reduced to a system of singular integral equations which can be accurately solved by using a numerical integration scheme based on Chebyshev polynomials. The M-integral is found to represent physically reasonable fracture behaviour and could serve as an effective measure for assessing damage due to single, multiple and slowly growing impermeable cracks. The applicability of mechanical energy release rate as a fracture criterion for magnetoelectroelastic solids is questionable as it shows behaviour very different from that predicted by the M-integral and total energy release rates for both single and multiple crack problems. On the other hand, the total energy release rate shows physically reasonable behaviour and good agreement with the M-integral when applied to the cases of single crack and horizontal double-crack systems. In the case of multiple cracks, crack tip parameters such as the total and mechanical energy release rates are generally not effective measures of global damage. Numerical results show an implicit relationship between the M-integral and effective elastic moduli of a medium with microcracks. Based on the M-integral, it is found that both positive and negative electric or magnetic loading generally inhibit crack propagation. In addition, crack orientation has significant influence on fracture parameters. Experimental studies will be required to identify a suitable fracture criterion for the present class of materials and will be useful in the validation of the theoretical models and in determining the adequacy of the different fracture criteria considered in this study.

Acknowledgements

Appendix A

The constitutive equations for x_2-polarized magnetoelectroelastic materials can be expressed as (Parton and Kudryavtsev, 1988),

$$
\begin{Bmatrix} \sigma_{11} \\ \sigma_{22} \\ \sigma_{33} \\ \sigma_{32} \\ \sigma_{31} \\ \sigma_{21} \end{Bmatrix} = \begin{bmatrix} C_{11} & C_{12} & C_{13} & 0 & 0 & 0 \\ C_{12} & C_{22} & C_{12} & 0 & 0 & 0 \\ C_{13} & C_{12} & C_{11} & 0 & 0 & 0 \\ 0 & 0 & 0 & C_{66} & 0 & 0 \\ 0 & 0 & 0 & 0 & \frac{1}{2}(C_{11}-C_{13}) & 0 \\ 0 & 0 & 0 & 0 & 0 & C_{66} \end{bmatrix} \begin{Bmatrix} \varepsilon_{11} \\ \varepsilon_{22} \\ \varepsilon_{33} \\ \varepsilon_{32} \\ \varepsilon_{31} \\ \varepsilon_{21} \end{Bmatrix} - \begin{bmatrix} 0 & e_{21} & 0 \\ 0 & e_{22} & 0 \\ 0 & e_{21} & 0 \\ 0 & 0 & e_{16} \\ 0 & 0 & 0 \\ e_{16} & 0 & 0 \end{bmatrix} \begin{Bmatrix} E_1 \\ E_2 \\ E_3 \end{Bmatrix} - \begin{bmatrix} 0 & h_{21} & 0 \\ 0 & h_{22} & 0 \\ 0 & h_{21} & 0 \\ 0 & 0 & h_{16} \\ 0 & 0 & 0 \\ h_{16} & 0 & 0 \end{bmatrix} \begin{Bmatrix} H_1 \\ H_2 \\ H_3. \end{Bmatrix}
$$

$$(A.1)$$

$$\begin{Bmatrix} D_1 \\ D_2 \\ D_3 \end{Bmatrix} = \begin{bmatrix} 0 & 0 & 0 & 0 & 0 & e_{16} \\ e_{21} & e_{22} & e_{21} & 0 & 0 & 0 \\ 0 & 0 & 0 & e_{16} & 0 & 0 \end{bmatrix} \begin{Bmatrix} \varepsilon_{11} \\ \varepsilon_{22} \\ \varepsilon_{33} \\ \varepsilon_{32} \\ \varepsilon_{31} \\ \varepsilon_{21} \end{Bmatrix} + \begin{bmatrix} \omega_{11} & 0 & 0 \\ 0 & \omega_{22} & 0 \\ 0 & 0 & \omega_{11} \end{bmatrix} \begin{Bmatrix} E_1 \\ E_2 \\ E_3 \end{Bmatrix} + \begin{bmatrix} \alpha_{11} & 0 & 0 \\ 0 & \alpha_{22} & 0 \\ 0 & 0 & \alpha_{11} \end{bmatrix} \begin{Bmatrix} H_1 \\ H_2 \\ H_3 \end{Bmatrix} \qquad (A.2)$$

$$\begin{Bmatrix} B_1 \\ B_2 \\ B_3 \end{Bmatrix} = \begin{bmatrix} 0 & 0 & 0 & 0 & 0 & h_{16} \\ h_{21} & h_{22} & h_{21} & 0 & 0 & 0 \\ 0 & 0 & 0 & h_{16} & 0 & 0 \end{bmatrix} \begin{Bmatrix} \varepsilon_{11} \\ \varepsilon_{22} \\ \varepsilon_{33} \\ \varepsilon_{32} \\ \varepsilon_{31} \\ \varepsilon_{21} \end{Bmatrix} + \begin{bmatrix} \alpha_{11} & 0 & 0 \\ 0 & \alpha_{22} & 0 \\ 0 & 0 & \alpha_{11} \end{bmatrix} \begin{Bmatrix} E_1 \\ E_2 \\ E_3 \end{Bmatrix} + \begin{bmatrix} \gamma_{11} & 0 & 0 \\ 0 & \gamma_{22} & 0 \\ 0 & 0 & \gamma_{11} \end{bmatrix} \begin{Bmatrix} H_1 \\ H_2 \\ H_3 \end{Bmatrix}. \qquad (A.3)$$

For plane strain deformations in the $x_1 x_2$ plane, the constitutive equations can be expressed as

$$\boldsymbol{\sigma} = \mathbf{C}\boldsymbol{\varepsilon} - \mathbf{e}^{\mathrm{T}}\mathbf{E} - \mathbf{h}^{\mathrm{T}}\mathbf{H}, \quad \mathbf{D} = \mathbf{e}\boldsymbol{\varepsilon} + \boldsymbol{\omega}\mathbf{E} + \boldsymbol{\alpha}\mathbf{H}, \quad \mathbf{B} = \mathbf{h}\boldsymbol{\varepsilon} + \boldsymbol{\alpha}\mathbf{E} + \boldsymbol{\gamma}\mathbf{H}, \qquad (A.4)$$

where

$$\boldsymbol{\sigma} = \begin{Bmatrix} \sigma_{11} \\ \sigma_{22} \\ \sigma_{12} \end{Bmatrix}, \quad \boldsymbol{\varepsilon} = \begin{Bmatrix} \varepsilon_{11} \\ \varepsilon_{22} \\ \varepsilon_{12} \end{Bmatrix}, \quad \mathbf{D} = \begin{Bmatrix} D_1 \\ D_2 \end{Bmatrix}, \quad \mathbf{E} = \begin{Bmatrix} E_1 \\ E_2 \end{Bmatrix}, \quad \mathbf{B} = \begin{Bmatrix} B_1 \\ B_2 \end{Bmatrix}, \quad \mathbf{H} = \begin{Bmatrix} H_1 \\ H_2 \end{Bmatrix} \qquad (A.5)$$

$$\mathbf{C} = \begin{bmatrix} C_{11} & C_{12} & 0 \\ C_{12} & C_{22} & 0 \\ 0 & 0 & C_{66} \end{bmatrix}$$

$$\mathbf{e} = \begin{bmatrix} 0 & 0 & e_{16} \\ e_{21} & e_{22} & 0 \end{bmatrix}, \quad \mathbf{h} = \begin{bmatrix} 0 & 0 & h_{16} \\ h_{21} & h_{22} & 0 \end{bmatrix}, \quad \boldsymbol{\omega} = \begin{bmatrix} \omega_{11} & 0 \\ 0 & \omega_{22} \end{bmatrix}, \quad \boldsymbol{\alpha} = \begin{bmatrix} \alpha_{11} & 0 \\ 0 & \alpha_{22} \end{bmatrix}, \quad \boldsymbol{\gamma} = \begin{bmatrix} \gamma_{11} & 0 \\ 0 & \gamma_{22} \end{bmatrix}. \qquad (A.6)$$

The Equations (A.4) and (A.5) are also valid for the plane stress case and the corresponding matrices $\mathbf{C}$, $\mathbf{e}$, etc can be easily derived from Equations (A.1) to (A.3).

References

Budiansky, B. and Rice, J.R. (1973). Conservation laws and energy-release rates. *ASME Journal of Applied Mechanics* **40**, 201–203.

Chen, Y.H. (2001a). M-integral analysis for two-dimensional solids with strongly interacting microcracks. Part I: in an infinite brittle solid. *International Journal of Solids and Structures* **38**, 3193–3212.

Chen, Y.H. (2001b). Conservation laws of the J_k-vector for microcrack damage in piezoelectric materials. *International Journal of Solids and Structures* **38**, 3233–3249.

Chen, Y.H. and Lu, T.J. (2003). Recent developments and applications of invariant integrals. *ASME Applied Mechanics Reviews*, **56**, 515–552.

Erdogan, F. (1978). Mixed boundary-value problem in mechanics. In Mechanics today (Edited by S. Nemat-Nasser), vol. **4**, pp. 1–86, Pergamon Press.

Erdogan, F. and Gupta, G.D. (1972). On the numerical solution of singular integral equations. *Quarterly Applied Mathematics* **29**, 525–534.

Fomethe, A. and Maugin, G.A. (1998). On the crack mechanics of hard ferromagnets. *International Journal of Non-Linear Mechanics* **33**, 85–95.

Gao, C.F., Kessler, H. and Balke, H. (2003a). Crack problems in magnetoelectroelastic solids. Part I: exact solution of a crack. *International Journal of Engineering Science* **41**, 969–981.

Gao, C.F., Kessler, H. and Balke, H. (2003b). Crack problems in magnetoelectroelastic solids. Part II: general solution of collinear cracks. *International Journal of Engineering Science* **41**, 983–994.

Gross, D. (1982). Spanungintensitatsfaktoren von ribsystemen (stress intensity factor of systems of cracks). *Ingenieur Archiv* **51**, 301–310.

Knowles, J.K. and Sternberg, E. (1972). On a class of conservation laws in linearized and finite elastostatics. *Archive for Rational Mechanics and Analysis* **44**, 187–211.

Liu, J.X., Liu, X.L. and Zhao, Y.B. (2001). Green's functions for anisotropic magnetoelectroelastic solids with an elliptical cavity or a crack. *International Journal of Engineering Science* **39**, 1405–1418.

Li, J.Y. (2000). Magnetoelectroelastic multi-inclusion and inhomogeneity problems and their applications in composite materials. *International Journal of Engineering Science* **38**, 1993–2011.

Lynch, C.S., Yang, W., Collier, L., Zuo, Z. and McMeeking, R.M. (1995). Electric field induced cracking in ferroelectric ceramics. *Ferroelectrics* **166**, 11–30.

Maugin, G.A. (1995). Material forces: Concepts and applications. *ASME Applied Mechanics Reviews* **48**, 213–245.

McHenry, K.D. and Koepke, B.G. (1983). Electric field effects on subcritical crack growth in PZT. *Fract. Mech. Ceram.* **5**, 337–352.

McMeeking, R.M. (2001). Towards a fracture mechanics for brittle piezoelectric and dielectric materials. *International Journal of Fracture* **108**, 25–41.

Miller, G.R. (1989). Analysis of cracks near interfaces between dissimilar anisotropic materials. *International Journal of Engineering Science* **27**, 667–678.

O' Handley, R.C. (2000). *Modern Magnetic Materials*. John Wiley, New York.

Pak, Y.E. (1992). Circular inclusion problem in antiplane piezoelectricity. *International Journal of Solids and Structures* **29**, 2403–2419.

Park, S.B. and Sun, C.T. (1995). Fracture criteria for piezoelectric ceramics. *Journal of American Ceramic Society* **78**, 1475–1480.

Parton, V.Z. and Kudryavtsev, B.A. (1988). *Electromagnetoelasticity*. Gordon and Breach Science Publishers, New York.

Rice, J.R. (1968). A path-independent integral and the approximate analysis of strain concentration by notches and cracks. *ASME Journal of Applied Mechanics* **35**, 379–386.

Sabir, M. and Maugin, G.A. (1996). On the fracture of paramagnets and soft ferromagnets. *International Journal of Non-Linear Mechanics* **31**, 425–440.

Shindo, Y. (1983). Dynamic singular stresses for a Griffith crack in a soft ferromagnetic elastic solid subjected to a uniform magnetic field. *ASME Journal of Applied Mechanics* **50**, 50–56.

Shindo, Y., Horiguchi, K. and Shindo, T. (1999). Magneto-elastic analysis of a soft ferromagnetic plate with a through crack under bending. *International Journal of Engineering Science* **37**, 687–702.

Shindo, Y. and Horiguchi, K. (2001). Magnetic fracture mechanics of ferromagnetic plates. *International Journal of Applied Electromagnetics and Mechanics* **15**, 275–281.

Singh, R.N. and Wang, H. (1995). Adaptive materials systems. (Edited by G.P. Carman, C. Lynch, N.R. Scottos), Proceedings of AMD-vol. 206/MD-vol. **58**, ASME, pp. 85–95.

Song, Z.F. and Sih, G.S. (2003). Crack initiation behavior in magnetoelectroelastic composite under in-plane deformation. *Theoretical and Applied Fracture Mechanics* **39**, 189–207.

Stroh, A.N. (1958). Dislocations and cracks in anisotropic elasticity. *Philosopical Magazine.* **7**, 625–646.

Suo, Z., Kuo, C.M., Barnett, D.M. and Willis, J.R. (1992). Fracture mechanics for piezoelectric ceramics. *Journal of the Mechanics and Physics of Solids* **40**, 739–76.

Tian, W.Y. and Chen, Y.H. (2002). Path-independent integral analyses for microcrack damage in dissimilar anisotropic materials. *Acta Mechanica* **154**, 101–120.

Ting, T.C.T. (1996). *Anisotropic Elasticity: Theory and Application*. Oxford Science, New York.

Xu, X.L. and Rajapakse, R.K.N.D. (2000). A theoretical study of branched cracks in piezoelectrics. *Acta Materialia* **48**, 1865–1882.